A COMPARISON OF THE AERODYNAMIC CHARACTERISTICS OF EIGHT

SAILWING AIRFOIL SECTIONS

Mark D. Maughmer*
Princeton University

SUMMARY

Because of its light weight, simple construction, and good aerodynamic performance, the Princeton sailwing may be a competitive alternative to conventional wings for many low-speed applications such as ultralight sailplanes, man-powered aircraft and high-performance hang gliders. The operational characteristics of the sailwing are discussed with some emphasis placed on the importance of the trailing-edge cable tension as it controls several aerodynamic properties. The three-dimensional aerodynamic characteristics of eight different sailwing profile sections have been obtained from wind tunnel tests and the results compared to determine the magnitude of the aerodynamic penalties paid for various structural simplifications. For the sectional thickness ratios considered in this research, it is concluded that, while the basic double-membraned sailwing has exceptional aerodynamic performance, even superior for some applications to the conventional hardwing, any notable deviation from this configuration results in an unacceptably large performance penalty.

INTRODUCTION

While there is currently a great deal of interest in the use of flexible wings for use on hang gliders, man-powered aircraft, and ultralight sailplanes, the design and evaluation of these vehicles is complicated a great deal by the fact that very little data is available to aid in analyzing the aerodynamic characteristics of such aircraft. Although the data presented herein was motivated by a National Science Foundation sponsored research program directed toward optimizing a windmill utilizing the Princeton sailwing, reference 1, it is hoped that these data will be of some value to designers of flexible-winged aircraft.

The Princeton sailwing, which has been under development since 1948, is a unique, semiflexible wing intended to provide the practical ultimate in a light-weight, low-cost lifting surface suitable for a number of low-speed applications. Basically, the structural configuration of the sailwing consists

---

*Currently with the Department of Aeronautical and Astronautical Engineering, University of Illinois, Urbana, Illinois.

of a leading-edge spar with attached ribs which ideally form a rigid framework supporting a trailing-edge cable in tension. A non-porous, non-stretchable cloth membrane, usually dacron, is then wrapped around the leading-edge and attached to the trailing-edge forming the upper and lower sail surfaces. The purpose of the pre-tensioned trailing-edge is to impart a chordwise tension in the membrane to minimize the deflections caused by the aerodynamic loads. Originally, it was not thought that the performance of such a device would compare favorably to that of a conventional wing; however, as a result of numerous experimental investigations, including those of reference 2, it has been found that the aerodynamic efficiency of the sailwing can indeed approach that of a hard wing.

Specifically, the data presented in this report were obtained as a result of a wind tunnel program which was undertaken and structured in such a manner as to ascertain the relative magnitude of the penalties associated with using a readily available circular cross-sectioned leading-edge as opposed to the D-section normally used in sailwing construction. In addition, the importance of the full double cloth membrane was explored by testing sailwing sections which did not utilize the lower membrane as well as several having only a partial lower membrane. In total, eight wings, identical in all respects except for the airfoil section utilized, were tested and compared.

In addition to the experimental development the sailwing has undergone, it should be noted that it has also received considerable analytical treatment such as that discussed in references 3-5.

SYMBOLS

b	Span
$\bar{c}$	Geometric mean chord
q	Dynamic pressure
t	Sectional thickness ratio
AR	Aspect ratio
C_D	Drag coefficient, Drag/qS
C_L	Lift coefficient, Lift/qS
C_M	Moment coefficient about the quarter-chord point of the geometric mean chord, $M/q\bar{c}S$
C_T	Trailing edge cable tension coefficient, $Tension/qb^2$
L/D	Lift-to-drag ratio
S	Wing area

MODEL DESCRIPTION

The tests of the eight different wing profiles, shown in figure 1, were performed in the Princeton University 1.2 m by 1.5 m force-balance wind tunnel. The wing planform utilized in this study is characterized by a span b of .96 m, a geometric mean chord $\bar{c}$ of .113 m, and a total area S of .108 square meters. The planform aspect ratio $AR = b^2/b\bar{c}$ is equal to 8.5. Relative to the length of the geometric mean chord, the sectional thickness ratio t is 11.5 percent. It was possible to adjust the tension of the trailing-edge cable in each of the models which, for the results discussed herein, was set at 42 N as well as 160 N. These settings yield a trailing-edge cable tension coefficient C_T of .07 and .28 respectively.

TEST CONDITIONS AND DATA REDUCTION

Most of the data collected in the series of experiments included in this report were obtained with the tunnel speed adjusted to yield a dynamic pressure q of 622.4 N/m^2. Although the corresponding Reynolds number based on the geometric mean chord is calculated to be approximately 230,000, because of the turbulence level in the tunnel, the aerodynamic data collected is considered to be qualitatively representative of a Reynolds number on the order of 750,000. In any case, the test results were obtained at a Reynolds number above the subcritical value for which laminar separation dominates and are therefore indicative of the operating conditions expected for somewhat higher Reynolds numbers.

The mounting of one of the test models in the wind tunnel is shown in figure 2. By means of an electrically driven tail-jack, it was possible to adjust the wing angle-of-attack to any value between -12 and +24 degrees while the tunnel was in operation. Thus, force balance data for lift, drag, and pitching moment were obtained at each two-degree angle increment between these limits. The test data were then reduced to the standard coefficient form and plotted as a function of the wing angle-of-attack as referenced to the unloaded (no-wind) orientation of the geometric mean chord, figures 5-8. In addition, the performance of each wing is summarized in a plot of lift-to-drag ratio as a function of lift coefficient, figures 9-10, and lift coefficient as a function of drag coefficient, figures 11-12.

CHARACTERISTICS OF THE SAILWING

Because many of the properties of the Princeton sailwing are uniquely different from those of a conventional hard wing, it is appropriate to discuss its operation to better understand the overall aerodynamic characteristics. For example, when the sailwing is at rest (no-wind), the cloth membrane is held taut by the trailing-edge cable and is essentially, except for the leading-edge, a symmetrical section as the upper and lower surfaces experience the same

pressure, figure 2. As the wing experiences airloads in a net lifting orientation (wind-on), the asymmetrical pressure distribution that is established between the upper and lower surfaces causes the membrane (or membranes) to displace away from the high pressure regions (underside) and move toward the low pressure regions (upperside). Thus, when a section is at an angle of attack greater than that of zero-lift, figure 3, it assumes a positive camber distribution that fairs the membrane in smoothly with the shape of the airfoil leading edge. It should be noted that the actual shape of the sailwing section is a function of the wind velocity, the angle-of-attack, the no-wind airfoil shape, and the amount of tension in the trailing-edge cable. Thus, as the angle-of-attack is increased, the resulting increased pressure differential between the upper and lower surfaces causes the amount of camber in the section to increase. This situation not only causes the maximum value of wing efficiency, the lift-to-drag ratio, to occur at relatively high lift coefficients, but also delays the impending stall. At this point, the importance of maintaining the desired trailing-edge cable tension should be noted. As might be expected, relaxing the cable tension allows a greater amount of camber to be established and therefore a higher maximum lift coefficient is obtainable; however, simultaneously, the maximum lift-to-drag ratio is decreased as well as the threshold of critical velocity at which detrimental sail luffing occurs. Thus, the amount of tension in the sailwing trailing-edge cable controls an important trade-off between the maximum lift coefficient and the maximum lift-to-drag ratio. It might be considered that as the cable tension becomes higher, the sailwing behavior is more like that of a rigid wing while as it becomes lower, the behavior approaches that of a high aspect ratio Rogallo wing.

Another interesting characteristic of the lifting sailwing is the upward deformation of the trailing-edge in the unsupported mid-span regions of each wing-panel, figure 4. The result of this action is a reduced angle of attack in these regions and one would expect a local reduction in lift; however, it is generally the case that this effect is more than offset by the increased amount of camber that occurs which results in a local increase in the generation to lift. In fact, because of this effect, the span lift distributions that occur over many of the sailwings that have been tested are often very close to that of the elliptical optimum.

The constant chordwise tension that is a result of the trailing-edge cable and the catenary-arc sail cut is responsible for many of the desirable features of the sailwing over other flexible designs. One such feature is that relatively low drags are present at low angles-of-attack and lift coefficients. Furthermore, unlike many flexible wing designs, the sailwing has the ability to pass smoothly through the zero-lift condition from that of a positive camber and lifting configuration to that of a negative camber and downward loading.

All in all, through many years of extensive research, the sailwing has been found to provide a simple, light-weight, and low-cost alternative to the conventional hard wing while not suffering any notable performance penalties throughout many low-speed applications.

PRESENTATION AND DISCUSSION OF TEST RESULTS

Representative three-dimensional lift, drag, and moment curves for four of the eight sailwing models tested are presented in the plots of figures 5-8. For each wing tested, the lift coefficient, drag coefficient, and pitching moment coefficient about the quarter-chord point, are plotted as a function of the angle-of-attack of the unloaded geometric mean chord. The lift-to-drag ratio as a function of lift coefficient for all of the sections tested are plotted in figures 9-10 while the drag polars, lift coefficient as a function of drag coefficient, are presented in figures 11-13. Finally, the typical effect of lowering the trailing-edge cable tension coefficient on the lift-to-drag ratio and the drag polar are shown in figures 14-15.

It is important to note that a direct comparison of these data to those of a conventional wing is complicated a great deal by the flexible nature of the sailwing. For example, the sailwing data can be likened to that of a rigid wing in which an automatic flap is deflected an additional amount for each incremental increase in angle-of-attack. This characteristic is responsible for the fact that it is generally impossible in the case of a sailwing to linearize the drag polar or obtain a meaningful value for the span-efficiency factor as is done from wind tunnel test data for a conventional wing. Similarly, it should further be noted that at lower angles-of-attack (up to approximately five degrees), it is not uncommon for a sailwing to have a lift-curve slope which significantly exceeds the theoretical thin airfoil maximum for rigid wings of 2π per radian. This occurs because the section is continually varying camber over the angle-of-attack range. At higher angles-of-attack, the section is unable to deform proportionally as much as it does when less loaded and, therefore, as the angle-of-attack is increased to higher values, the lift-curve becomes increasingly more like that of a rigid wing.

The most notable observation in comparing the compilation of data presented in figures 9-12 is the significant performance advantage held by the conventional, double-membraned version tested over the more simplified versions. This advantage is so great that it is inconceivable of a situation in which the potential benefit in weight saving, cost, or more-simplified construction for any of the modified versions could be justified in relation to the performance penalties.

Examination of these data further indicate an important feature in that the sailwing highest L/D values occur in a range of relatively large values of lift coefficient. Furthermore, the flexible nature of the sailwing affords it low drag coefficient values over a relatively wide range of lift coefficients, particularly in the case of the double-membraned sections.

In order to further emphasize the fact that unlike a conventional wing, the shape of the sailwing section is governed by the dynamic pressure (wind velocity), a polar for sailwing model 2 is shown in figure 13 for the case of a constant wing loading. This polar was obtained by adjusting the tunnel velocity such that the lift force remained constant throughout the angle-of-attack range and is representative of the aerodynamic characteristics over the

speed range of an aircraft in level flight where the load factor is equal to unity. Thus, the high-speed flight conditions correspond to the lower lift coefficients while the low-speeds correspond to lift coefficients approaching the maximum value at stall. For comparison, the constant velocity polar of sailwing model 2 is also shown in figure 13. The difference between these two plots, excepting for the small contribution due to the changing Reynolds number over the speed range for the constant wing loading case, can be attributed to the flexible nature of the sailwing. For an equivalent hard wing, one would expect these two plots to be nearly identical. From the figure, it should be noted that the sailwing maximum lift-to-drag ratio of twenty, corresponding to the tangent to the curve drawn from the origin, occurs at a fairly high lift coefficient and that the operating range of low drag values is fairly wide. It is important to note, however, that in order to maintain a suitably high test Reynolds number these data were collected at a wing loading of 598 N/m^2 which is relatively high for most motorless applications. More practical wing loadings would cause the maximum lift-to-drag ratio to correspond to slightly lower lift coefficient values.

In attempting to generalize the effect of the different leading edge shapes employed, it is apparent that those sections having the smaller radius version have a wider region of low drag although, for the most part, the actual minimum values of the drag coefficient are slightly lower for the more rounded leading edge shape. Furthermore, as expected, the more pointed cross-section is accompanied by more abrupt stalling characteristics. Lastly, particular attention should be paid to the comparatively poor performance delivered by the often employed circular leading edge.

The effects of lowering the trailing edge cable tension are as expected and summarized by the data plotted in figures 14 and 15. Briefly a reduction of the trailing edge cable tension leads to a higher value of the lift curve slope, gentler stalling characteristics, a higher value of the maximum lift coefficient, and a generally lower value of the maximum lift-to-drag ratio; however, it should be noted, as observed in figure 14, that the lower trailing edge cable tension results in larger lift-to-drag ratios occurring in the region near the maximum lift coefficient.

CONCLUSIONS

In reviewing the applicability of the data presented herein, it should be born in mind that the quantitative information becomes less valid as deviation occurs from the equivalent test Reynolds number; however, as the test condition is above that of the critical Reynolds number, the trends, relationships, and approximate values of the data should remain valid to somewhat higher values. In addition, note that the sectional thickness ratios employed for those tests are somewhat higher than those used on many current hang gliders and should be taken into account when contemplating the use of these test results. In particular, it is expected that the importance of the leading edge shape should diminish as the thickness ratio decreases and the circular leading edge shape should prove adequate, as it often has, for some applications.

In considering the findings of these tests in addition to many others, it has been demonstrated that the three-dimensional performance of the Princeton sailwing is quite competitive with many hard wings of the same aspect ratio. Thus, the use of the sailwing should allow the benefits of simpler construction and lower costs to be realized without paying any significant price in performance. In fact, some consideration should be given to the fact that, unlike many of its rigid counterparts, the cambering characteristics found in the sailwing cause its three-dimensional lift-to-drag ratio to maximize at a fairly high lift coefficient as is desirable for many of the low-speed applications for which the sailwing is suitable. Furthermore, relative to many conventional wing sections, the sailwing has the favorable characteristic of a fairly slow rise in the drag coefficient, and consequently a slow decrease in the lift-to-drag ratio, with increasing values of the lift coefficient.

If one's mind is allowed to freely extrapolate from current trends and the results of this test program, one can envision the reality of a ultralight sailwing sailplane in which a cockpit lever is used to vary the wing trailing edge cable tension. Thus, in operation similar to that of a modern flapped sailplane, the pilot would slacken the cable upon entering a thermal to permit a slow tight circle with a high value of lift coefficient and upon exiting the thermal, pushes the lever to tighten the cable such that a high lift-to-drag ratio for inter-thermal cruise is obtained. Perhaps in the not too distant future, an aircraft of this type might bridge the gap between the limitations of hang gliding and the excessive costs of high performance.

REFERENCES

1. Maughmer, M. D. "Optimization and Characteristics of a Sailwing Windmill Rotor." NSF/Rann/GI-41891/PR/75/4, Princeton University AMS Report No. 1297, July 1976.

2. Fink, M. P. "Full-Scale Investigation of the Aerodynamic Characteristics of a Model Employing a Sail-Wing Concept." NASA Technical Note TN D-4062, July 1967.

3. Ormiston, R. A. "Theoretical and Experimental Aerodynamics of an Elastic Sailwing." Department of Aerospace and Mechanical Sciences, Princeton University, Ph.D. Dissertation, October 1969.

4. Ormiston, R. A. "Theoretical and Experimental Aerodynamics of the Sailwing." Journal of Aircraft, Vol. 8, No. 2, February 1971, pp. 77-84.

5. Mercer, J. E. "Steady and Unsteady Aerodynamics of an Elastic Sailwing: Theory for Design." Department of Aerospace and Mechanical Sciences, Princeton University, Ph.D. Dissertation, April 1970.
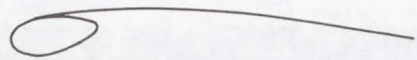
Sailvane Model 1   Semi-Sailwing Model 1   Sailwing Model 1
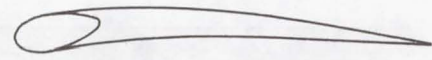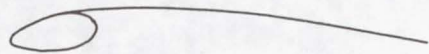
Sailvane Model 2   Semi-Sailwing Model 2   Sailwing Model 2
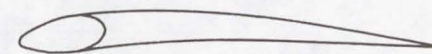
Sailvane Model 3   Semi-Sailwing Model 3

Figure 1.- Sailvane and sailwing sections tested.
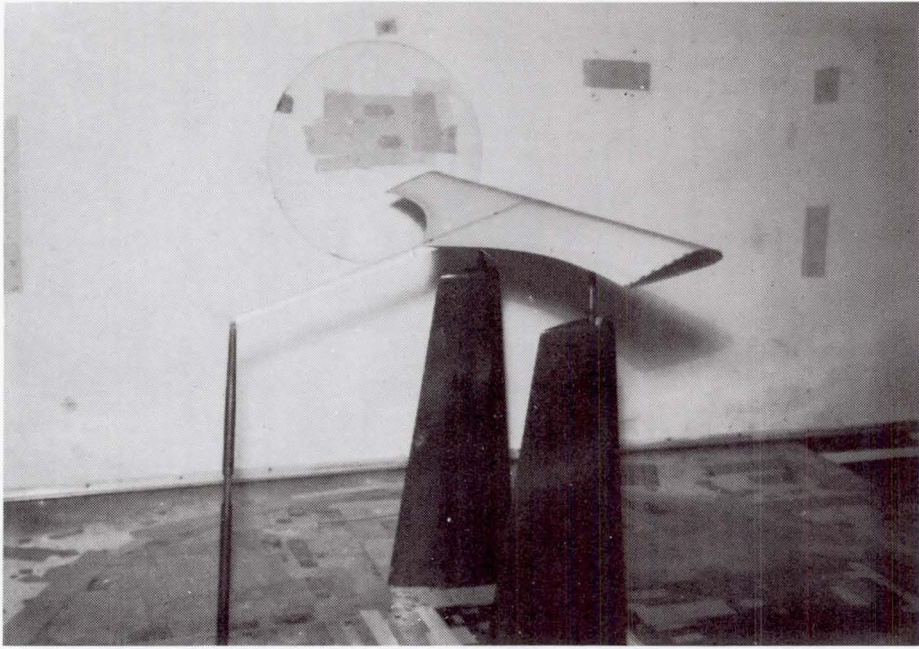
Figure 2.- Typical sailwing model mounted in
wind tunnel with wind off.
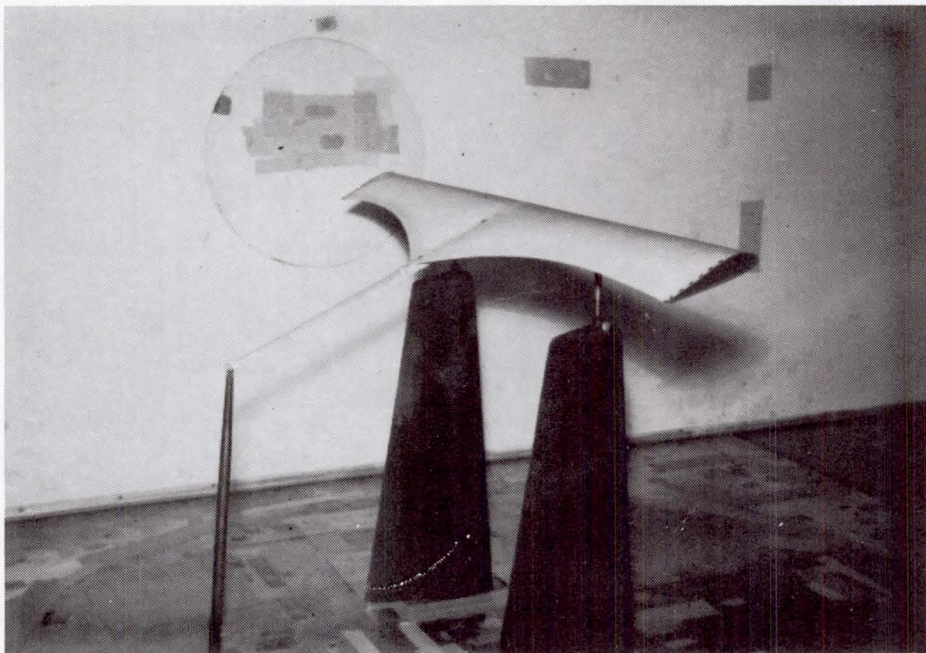
Figure 3.- Sailwing mounted in wind tunnel
with wind on.
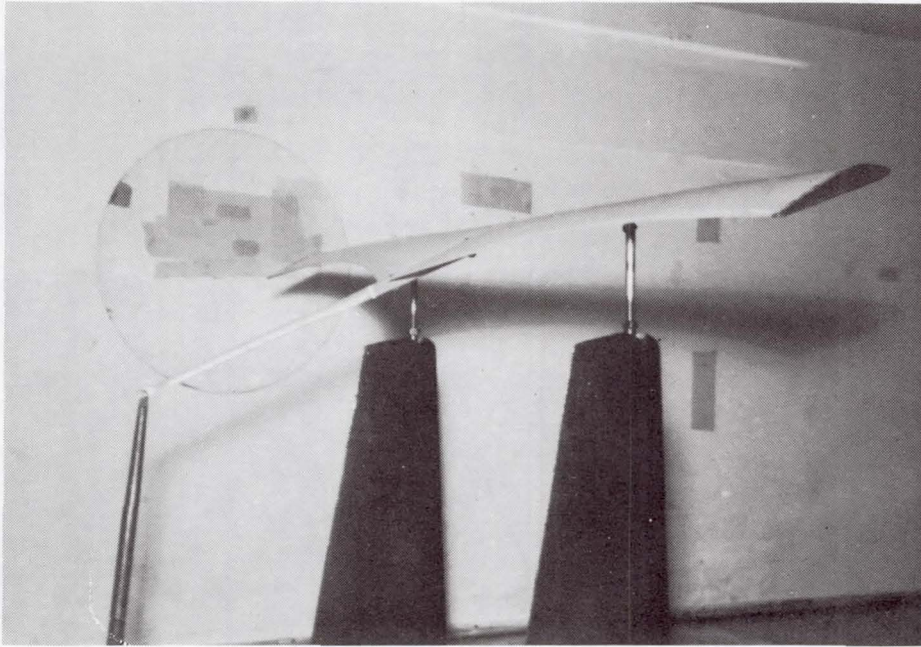
Figure 4.- Detail of sailwing trailing edge deformations.
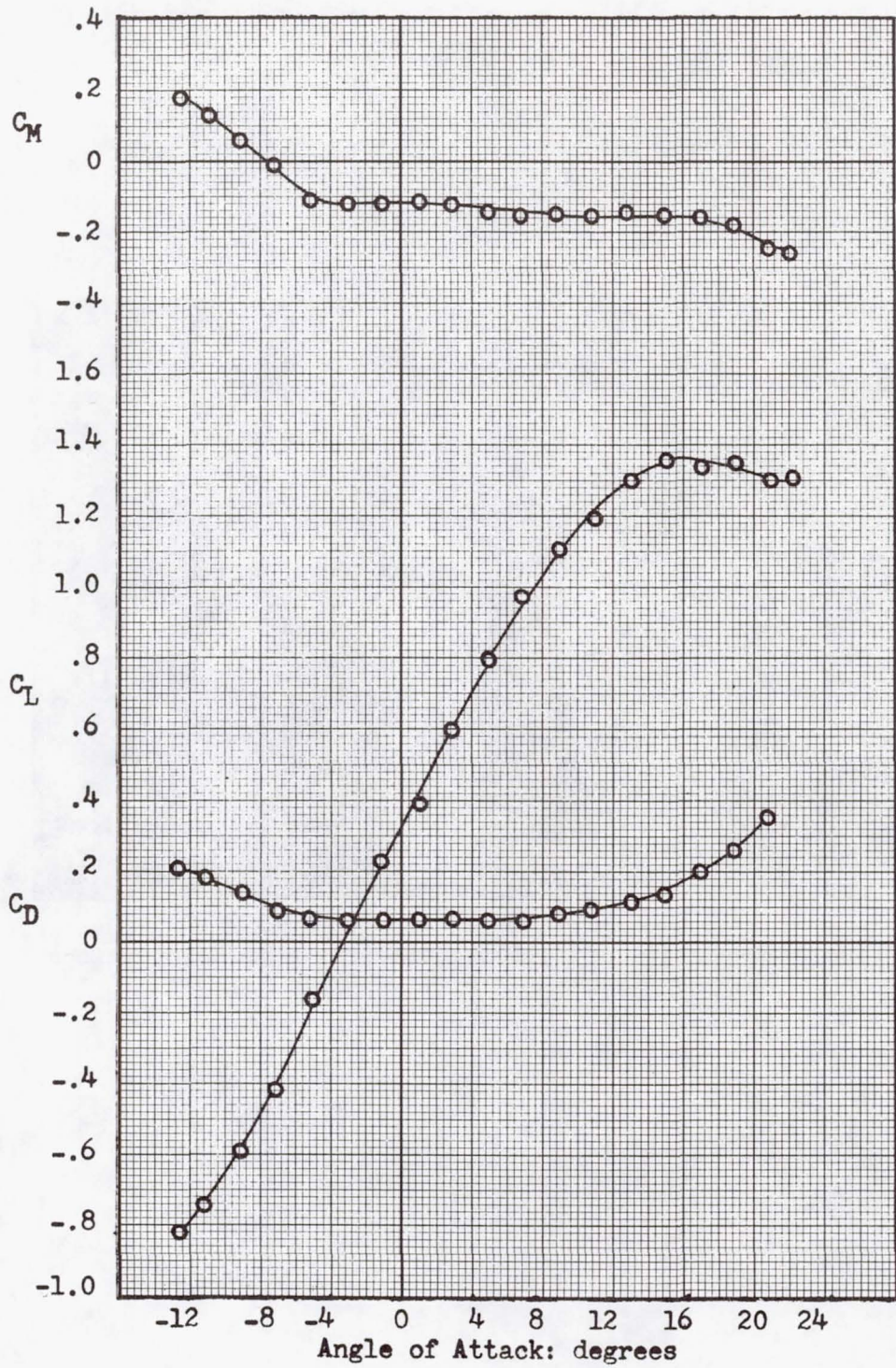
Figure 5.- Aerodynamic characteristics of the sailvane model 2.

Figure 6.- Aerodynamic characteristics of the semi-sailwing model 2.
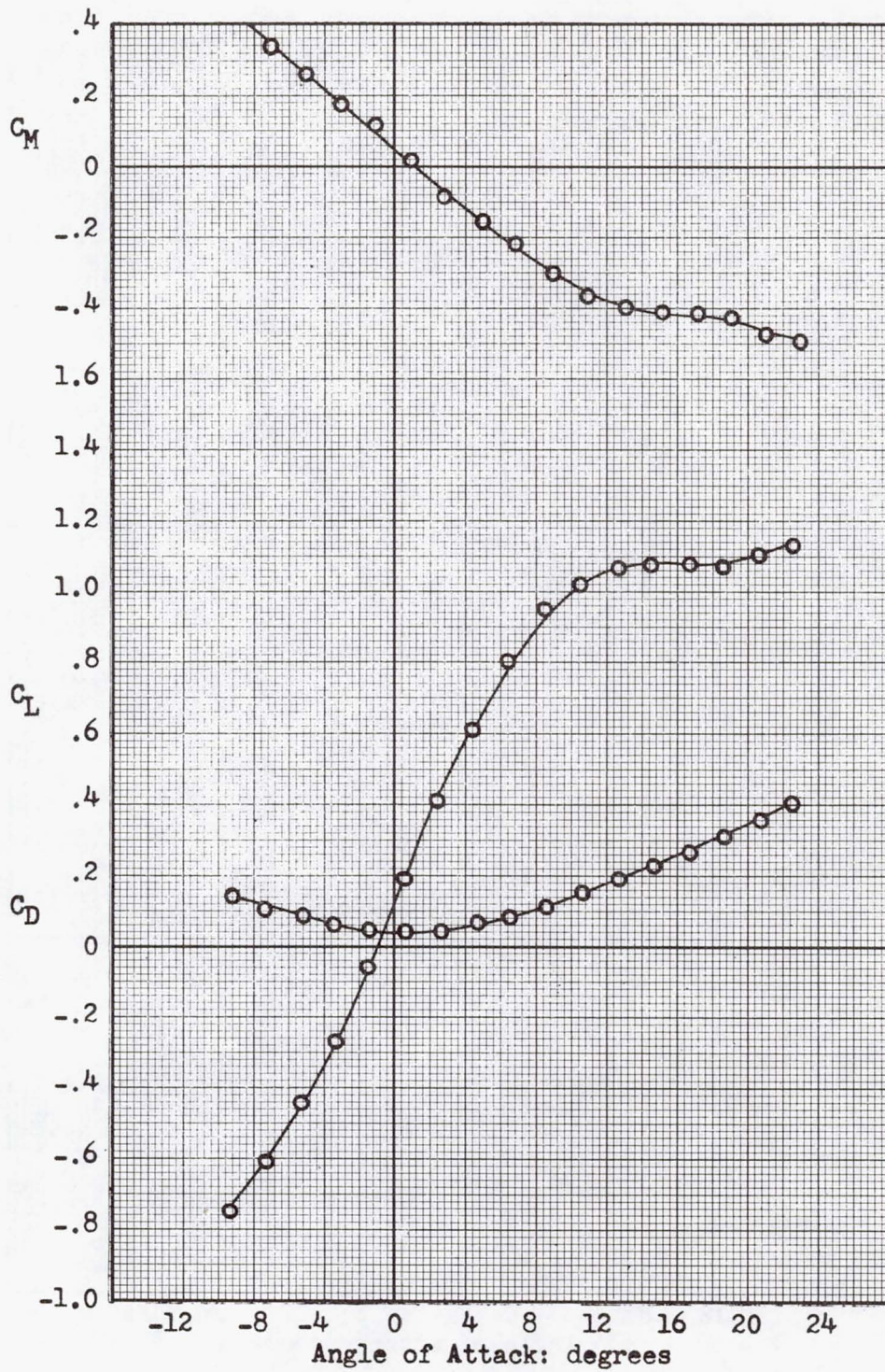
Figure 7.- Aerodynamic characteristics of the semi-sailwing model 3.
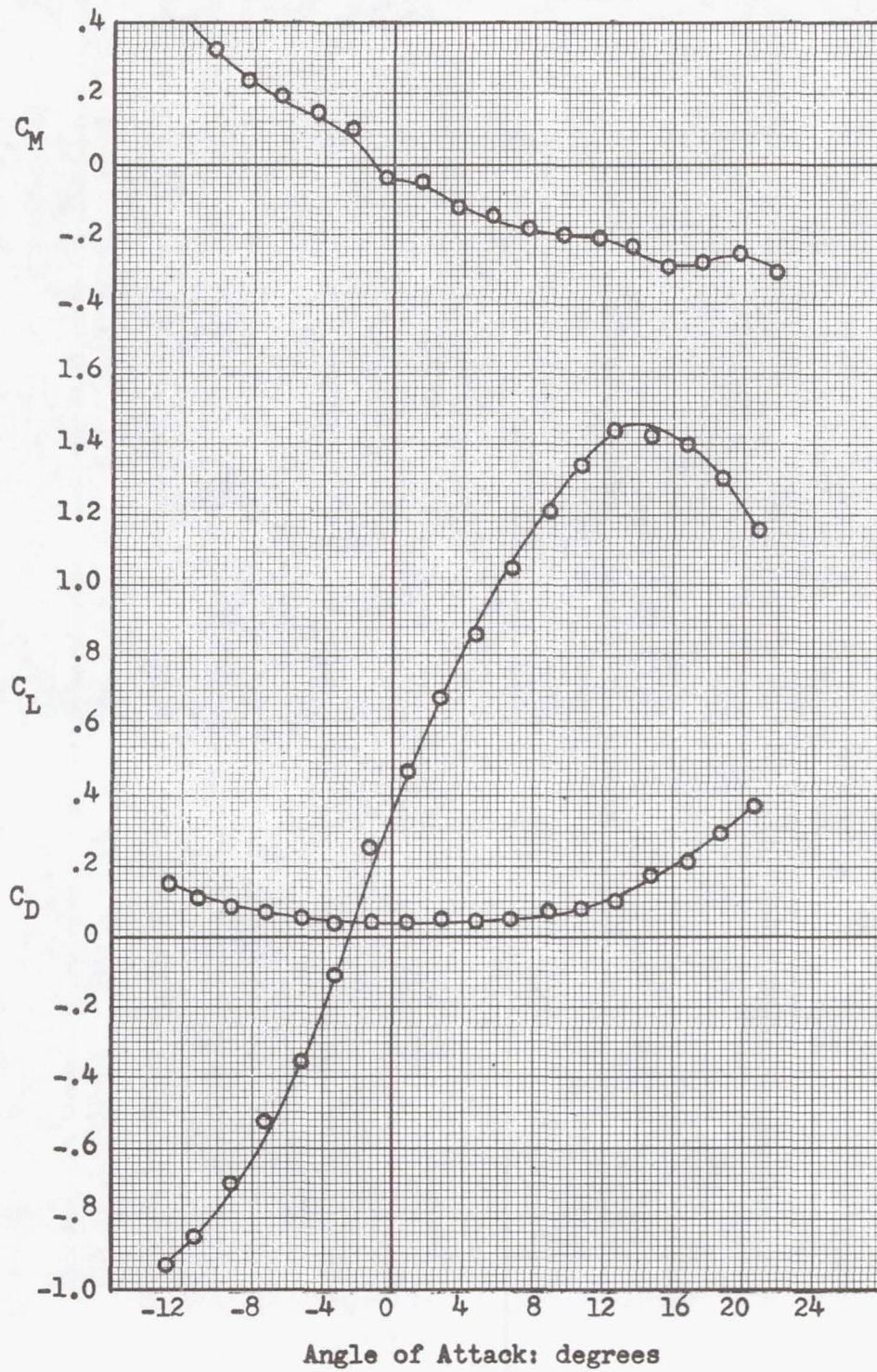
Figure 8.- Aerodynamic characteristics of the sailwing model 2.
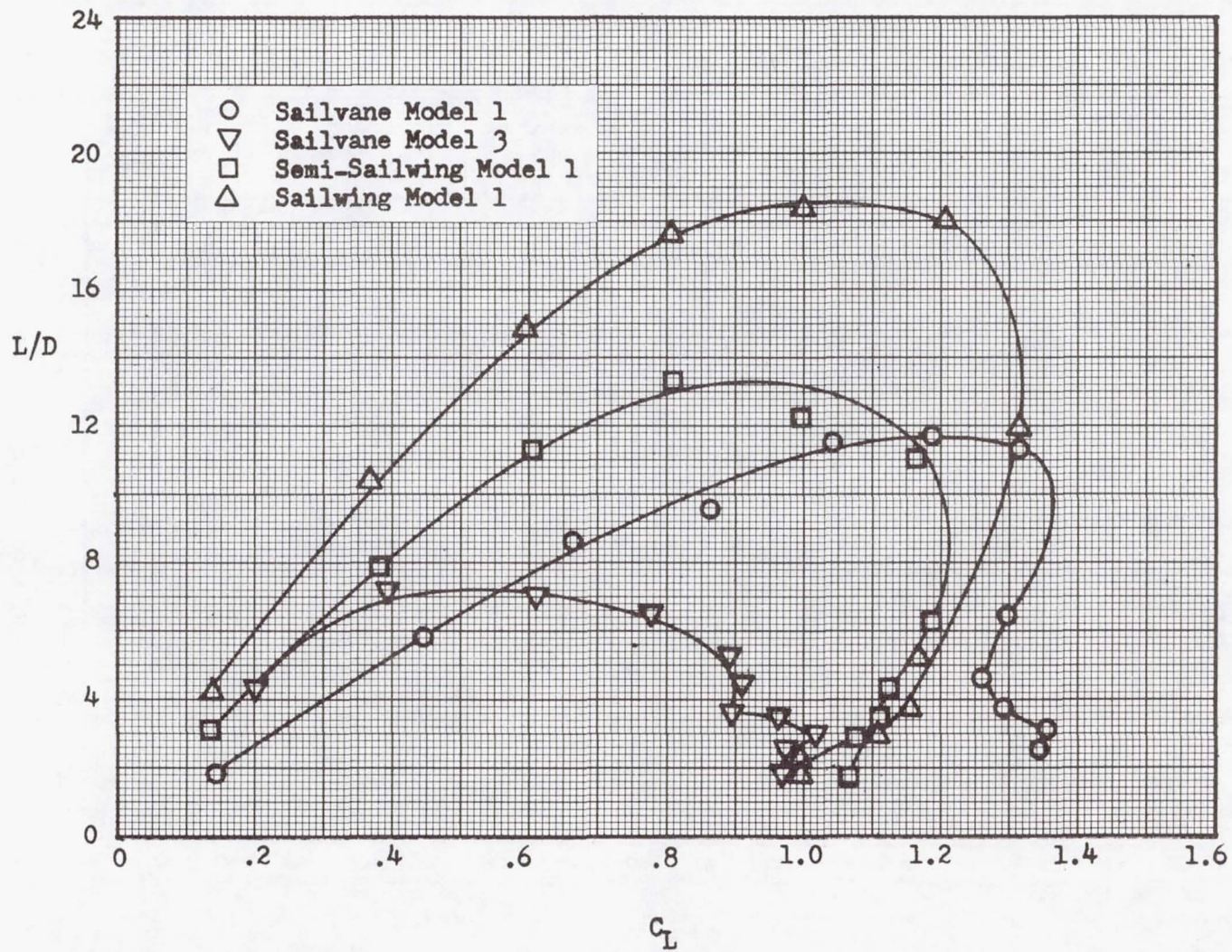
Figure 9.- Composite L/D vs. C_L plot of sailwings with the larger radius leading-edge.
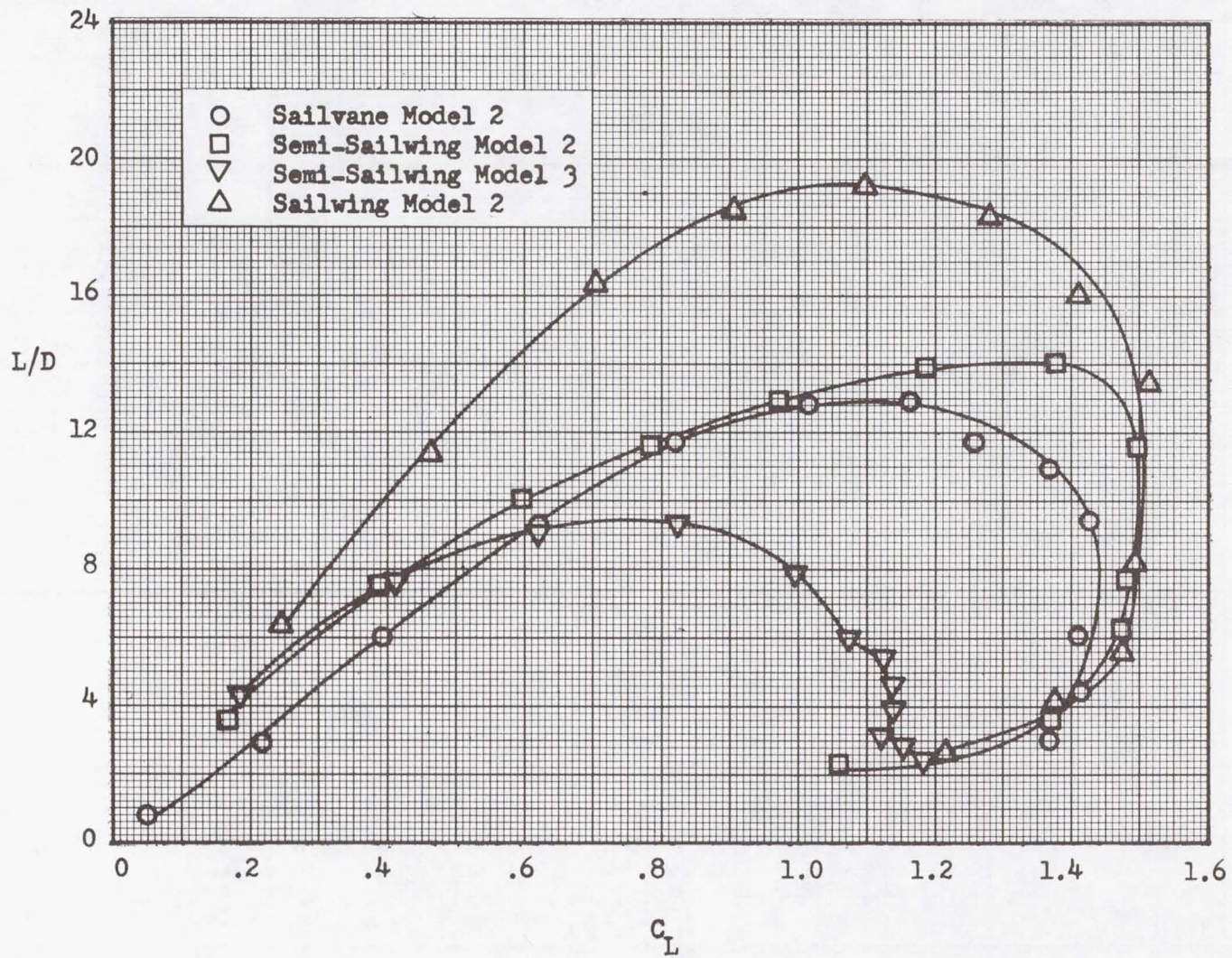
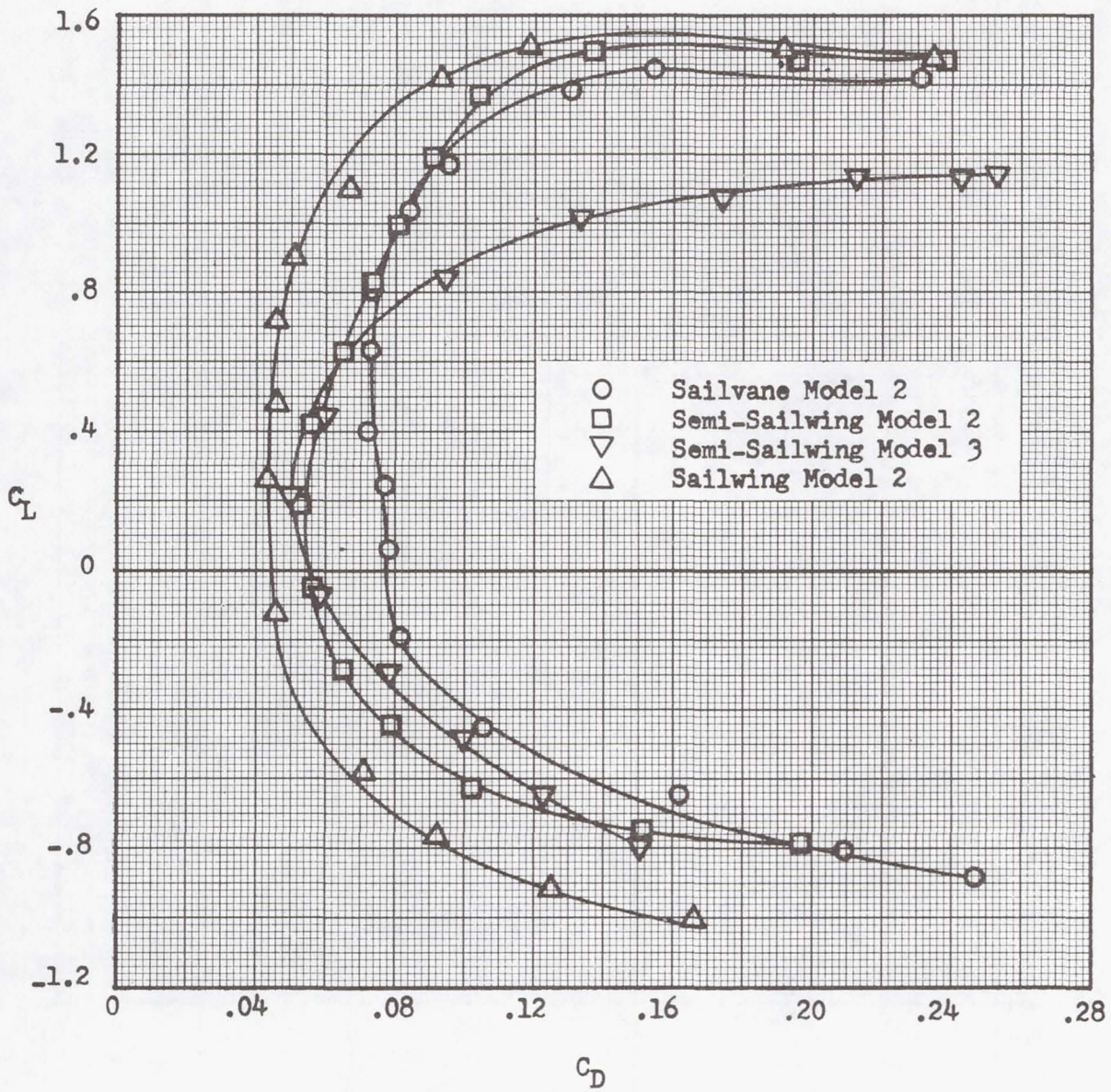Figure 10.- Composite L/D vs. C_L plot of sailwings with the smaller radius leading-edge.
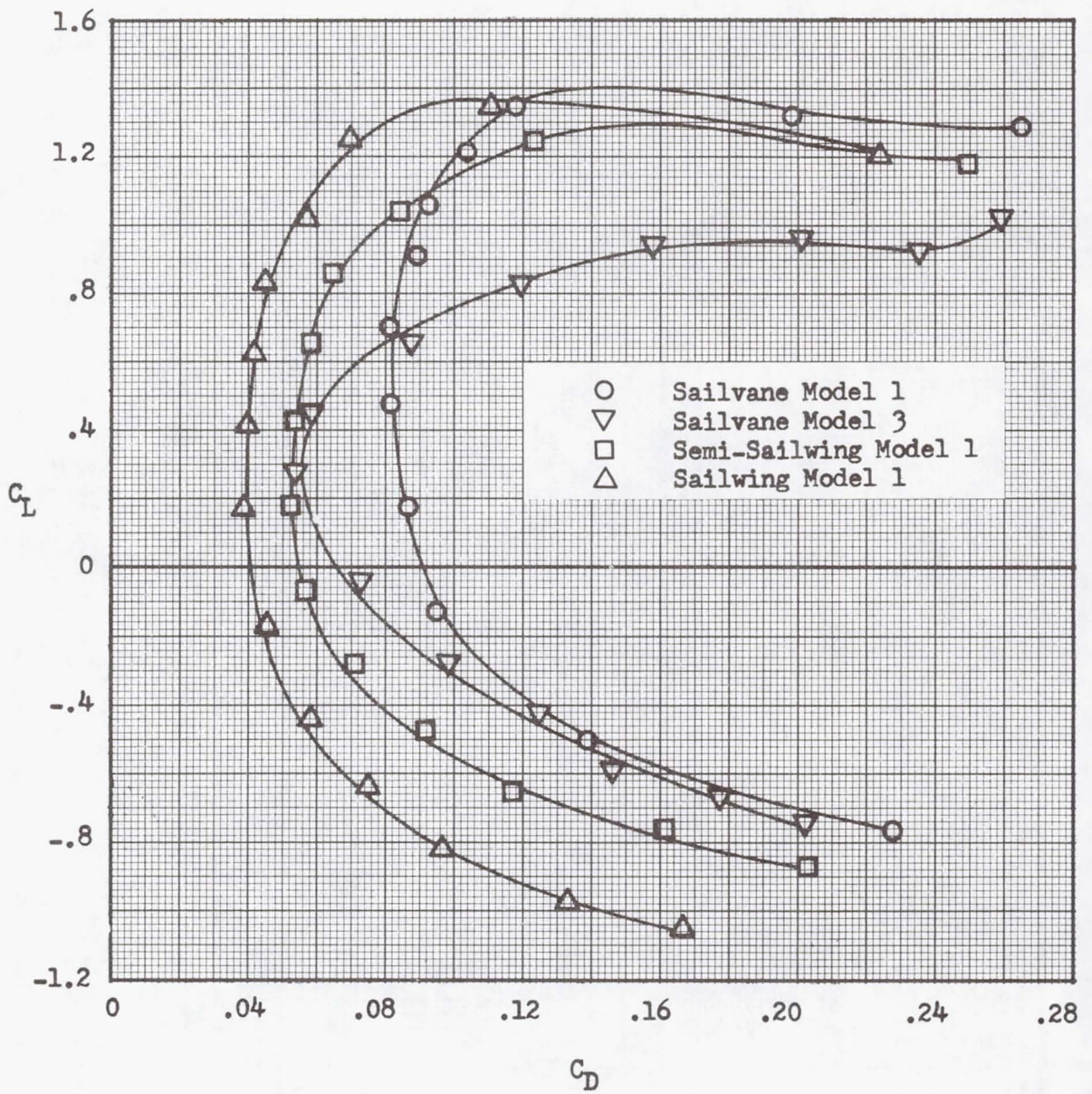
Figure 11.- Composite polar plot of sailwings with the
larger radius leading-edge.

Figure 12.- Composite polar plot of sailwings with the
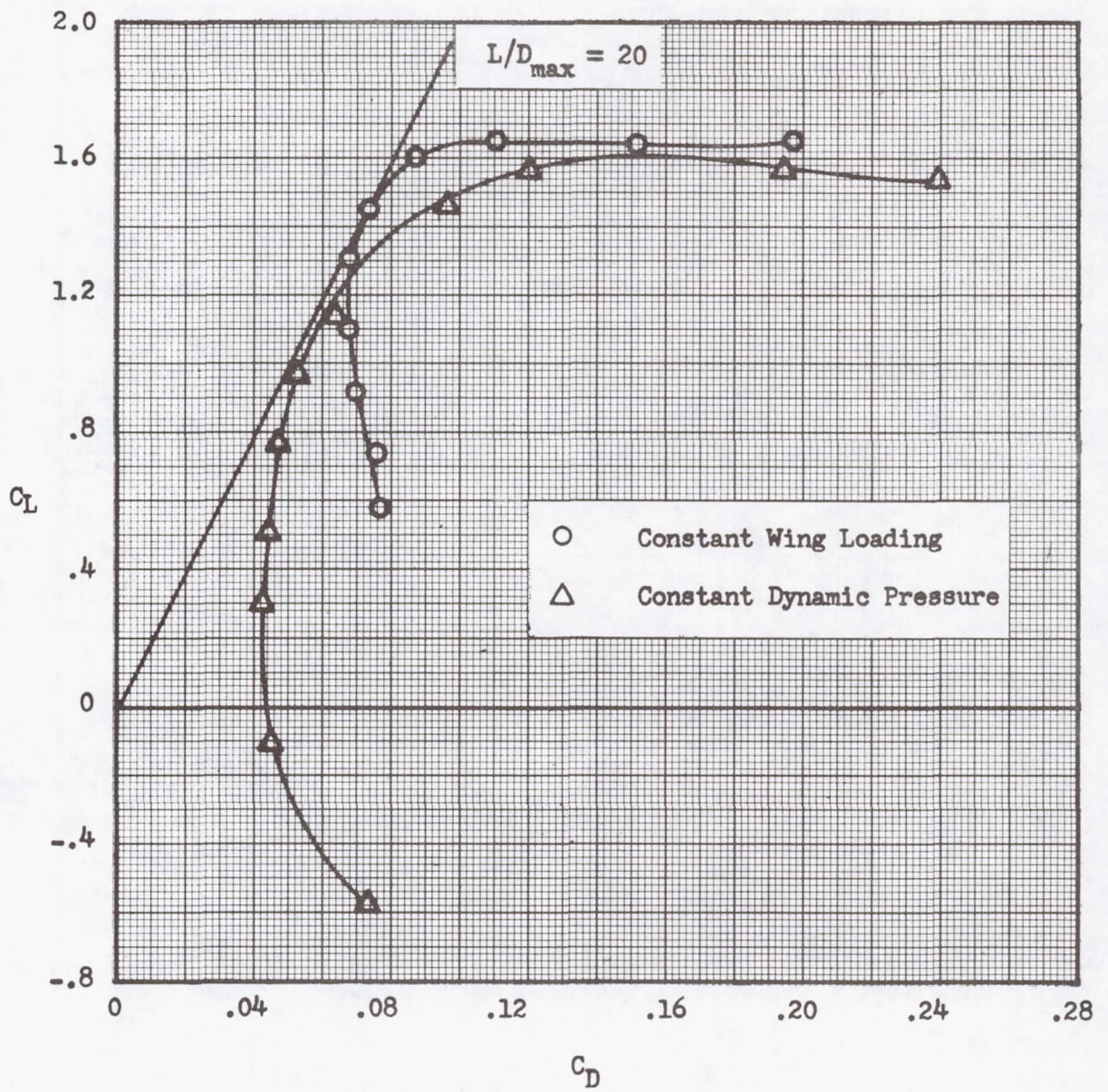smaller radius leading-edge.

Figure 13.- Sailwing model 2 constant wing loading drag polar compared
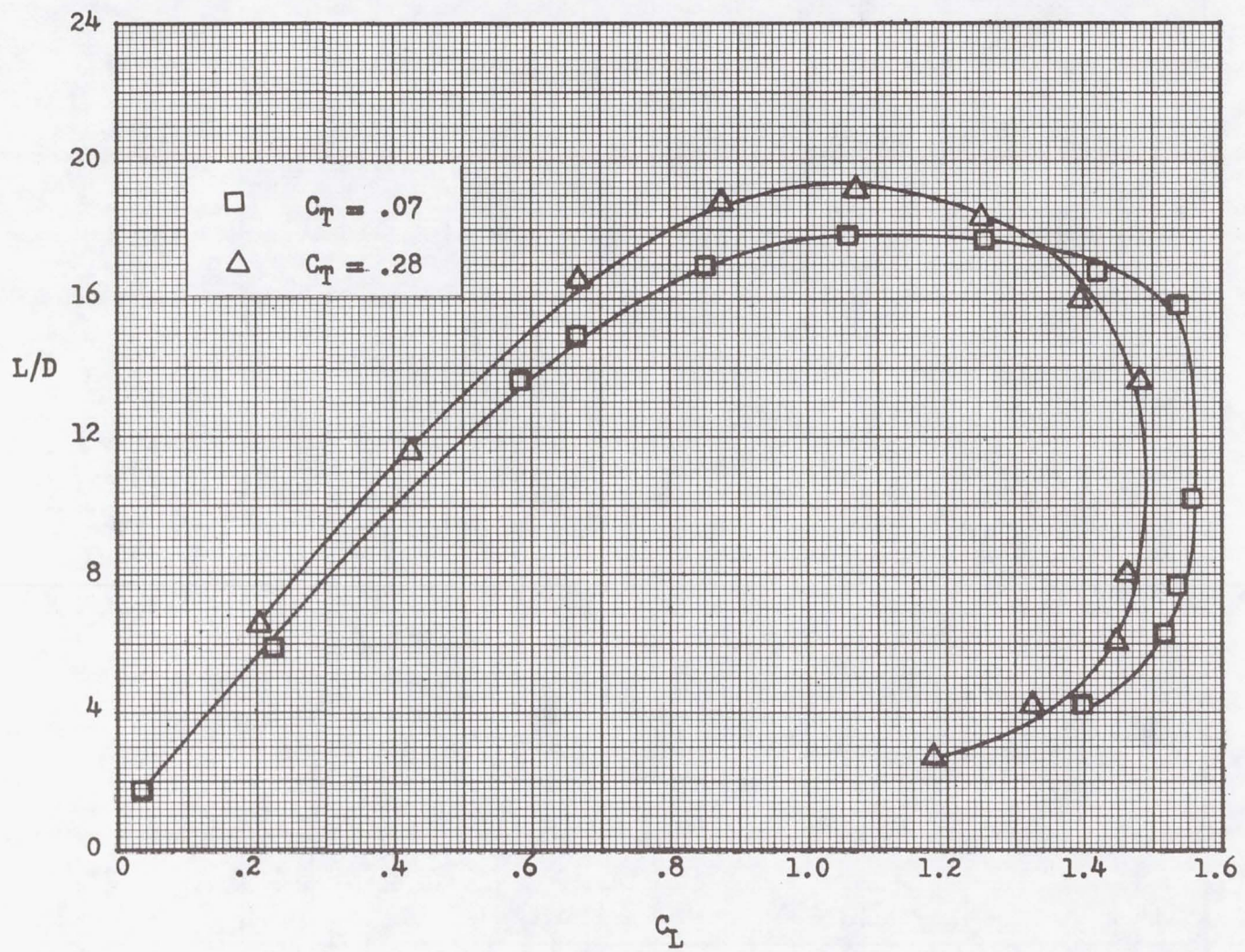to the constant dynamic pressure drag polar.

Figure 14.- Effect of sailwing trailing-edge cable tension on
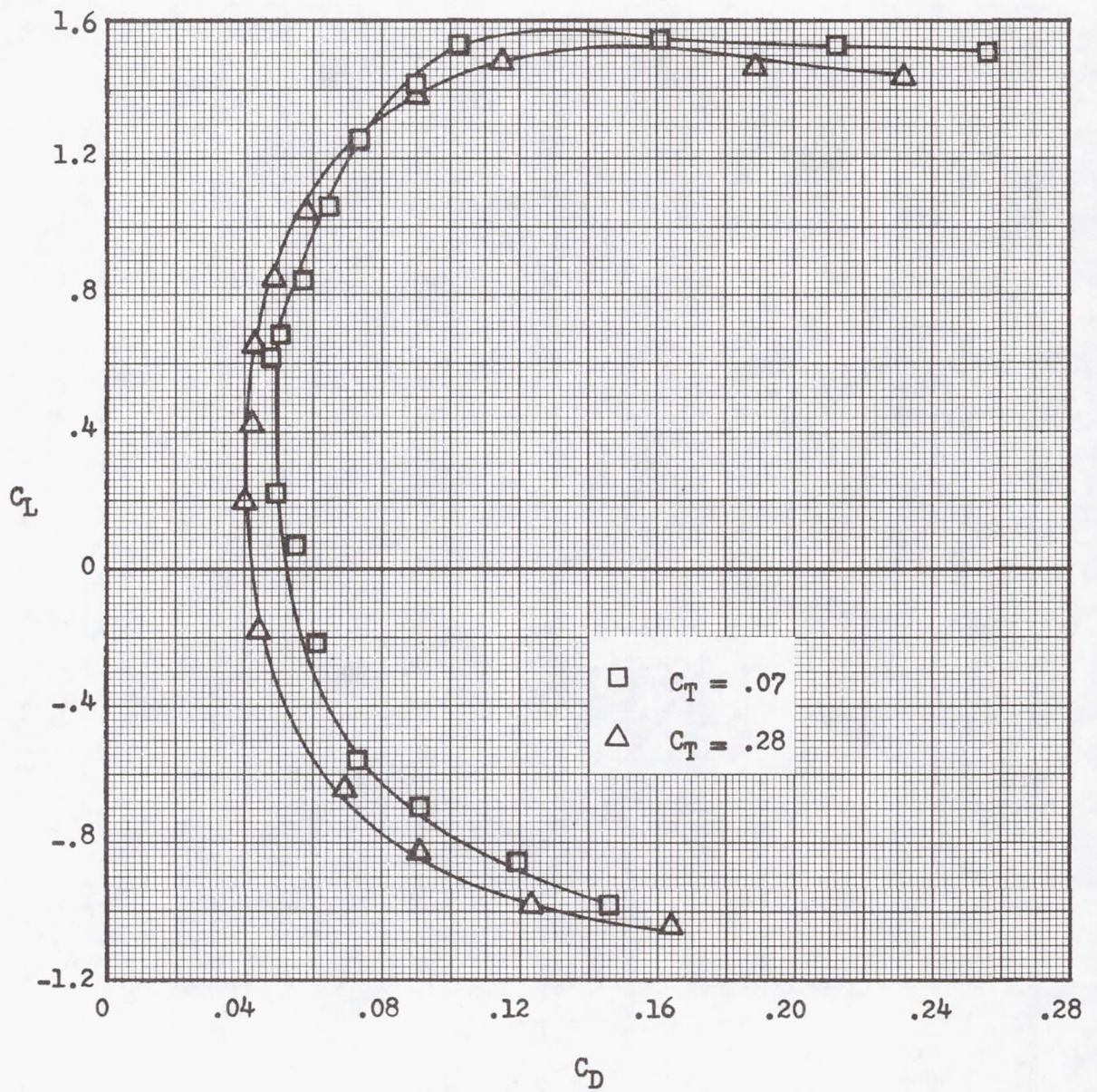lift-to-drag ratio: sailwing model 2.

Figure 15.- Effect of sailwing trailing-edge cable tension on the drag polar: sailwing model 2.